Commun Nonlinear Sci Numer Simulat 32 (2016) 1–9

Contents lists available at ScienceDirect

Commun Nonlinear Sci Numer Simulat

journal homepage: www.elsevier.com/locate/cnsns

Modulational instability of the Kuznetsov-Ma breather in optical fibers with constant and periodic dispersion

U. Al Khawaja [a,*], S.M. Al-Marzoug [b,c], H. Bahlouli [b,c], F.Kh. Abdullaev [d]

[a] Physics Department, United Arab Emirates University, P.O. Box 15551, Al-Ain, United Arab Emirates
[b] Physics Department, King Fahd University of Petroleum and Minerals, Dhahran 31261, Saudi Arabia
[c] Saudi Center for Theoretical Physics, Dhahran 31261, Saudi Arabia
[d] Department of Physics, Kulliyyah of Science, International Islamic University of Malaysia, Bandar Indera Mahkota, Kuantan 25200, Pahang, Malaysia

ARTICLE INFO

Article history:
Received 26 March 2015
Revised 22 June 2015
Accepted 25 July 2015
Available online 12 August 2015

PACS:
05.45.Yv
03.75.Lm
05.30.Jp

Keywords:
Kuznetsov-Ma breather
Modulational instability

ABSTRACT

We perform modulational instability analysis of the Kuznetsov-Ma breather (KMB) propagating in a medium with constant and periodic dispersions. In the constant dispersion case, we show that the most unstable modulational instability eigenmode leads to bifurcation of the KMB into a sequence of breathers. The time at which bifurcation starts and the bifurcation rate are quantitatively accounted for. In the case of a KMB propagating in an optical fiber with a constant dispersion perturbed by a sinusoidal time-dependent modulation our results suggest that the KMB is most unstable just before and after the breather reaches its maximum peak height. Parametric resonance occurs when the frequency of the dispersion modulation is much larger than the natural frequency of the breather.

1. Introduction

Over the past few years breathers over a finite background have been proposed as models for rogue waves in ocean [1] and have been observed in optical systems [2]. These comprise, the Akhmediev breather (AB), a solution that is periodic in space and localized in time [3], the Kuznetsov-Ma breather (KMB), a solution that is periodic in time and localized in space [4], and finally the Peregrine soliton which is localized in both time and space [5]. The Peregrine soliton models a wave that appears at a specific time and space but disappears almost suddenly while its maximum amplitude can reach three times the amplitude of the unperturbed wave. For these special features, the Peregrine soliton have been considered as special prototype of freak waves [6]. The Peregrine soliton has been recently reproduced experimentally in wave tank laboratories [7] and in optical fibers [8]. Recent experiments have also reported the evidence of Peregrine solitons in plasmas [9]. Nonetheless, AB and KMB can be also considered as models for rogue waves since they correspond to a large-amplitude wave over a finite background. Furthermore, both breathers are connected to the Peregrine soliton through a limiting procedure. Indeed the KMB has been realized experimentally in optical fibers [10]. Stability of the three breathers is thus worth studying since it will shed some light on the stability of rogue waves. In [11] authors have studied the stability of the AB. In our recent work [12], we have studied the stability of the Peregrine soliton. Completeness thus warrants studying the stability of the KMB.

* Corresponding author. Tel.: +97137136335.
E-mail address: u.alkhawaja@uaeu.ac.ae (U. Al Khawaja).

http://dx.doi.org/10.1016/j.cnsns.2015.07.012
1007-5704/

Modulational instability (MI) of the constant-wave solution (CW) in optical fibers with periodic dispersion was investigated in Refs. [13,14] and has recently been observed [15,17]. There is, however, a fundamental difference between MI of CW and that of the KMB. In contrast with CW, both the phase and profile of the KMB are time-dependent in a nontrivial manner. In MI, small perturbations of a given solution grow exponentially with time leading to an instability that is usually a sign on the formation of another solution. This is, for instance, the case with sinusoidal spatial perturbations on top of the CW solution leading to the AB. The time dependence of KMB interferes with that of the perturbations. Therefore, MI predictions will be valid only when the growth rate of the perturbations is considerably larger than the natural time rate at which the KMB evolves. Under this restriction we will use in the present work the MI analysis to study two main features of the KMB, namely its *bifurcation* and *parametric resonance*. Bifurcation of the KMB is observed when one solves numerically the governing nonlinear Schrödinger equation (NLSE) where the KMB bifurcates at a certain time into two breathers which in turn bifurcate further leading to an inverted triangular-shaped structure in the time-space domain (see e.g. Figs. 2 and 9 below). We will show that this specific pattern is generated by the most unstable eigenmode of the MI of the KMB. In the case of a periodically-modulated dispersion, it is expected that parametric resonance takes place between the frequency of the modulation and the natural frequency of the KMB where the peaks of the breather will be either boosted or suppressed by the periodic dispersion. This will be evident by studying the effect of the parameters of the periodic dispersion, namely its frequency and amplitude, on the growth rate of the most unstable eigenmodes.

The paper is organized as follows. In Section 2 we introduce the model, governing equations and formulate the problem at hand. In Section 3, we apply the MI analysis to study in Section 3.1 the bifurcation of the KMB and in Section 3.2 the parametric resonance. The paper is then concluded in Section 4 with a summary of the main results.

2. Theoretical model

The propagation of the KMB along a dispersion-managed fiber is governed by the dimensionless attractive nonlinear Schrödinger equation

$$i\,\frac{\partial}{\partial t}\Psi(x,t) = -\frac{d(t)}{2}\,\frac{\partial^2}{\partial x^2}\Psi(x,t) - |\Psi(x,t)|^2\,\Psi(x,t) \tag{1}$$

where

$$d(t) = d_0 + d_1\,\sin(\omega_0\,t) \tag{2}$$

with $d_{0,\,1}$ being constants. The KMB is an exact solution of Eq. (1) with $d_0 = 1,\ d_1 = 0$, which reads

$$\psi_{\mathrm{KMB}}(x,t) = \sqrt{2}\,e^{2\,i\,t}\left[\frac{\cos(\Omega\,t - 2\,i\,\phi) - \cosh(\phi)\,\cosh(\sqrt{2}\,p\,x)}{\cos(\Omega\,t) - \cosh(\phi)\,\cosh(\sqrt{2}\,p\,x)}\right], \tag{3}$$

where $\Omega = 2\,\sinh(2\,\phi)$ and $p = 2\,\sinh(\phi)$. Here ϕ is an arbitrary real parameter. We denote, here and throughout, the frequency Ω as the *natural* frequency of the fundamental KMB, as it gives the frequency of peak appearance. Furthermore, we define $T = 2\pi/\Omega$ as its period. In Section 3.1, we perform the MI analysis of this solution for constant dispersion, $d_0 = 1$ and $d_1 = 0$, and then in Section 3.2 the MI analysis is performed in the presence of the time-dependent dispersion, $d_1 \neq 0$.

It should be noted from the outset that the time dependence of the KMB requires special treatment when the dispersion is also time-dependent. A conventional effective time-dependent approach was discussed and described in detail in our previous work [12]. We outline here the main steps of the calculation for completeness. Consider the perturbed solution

$$\Psi(x,t) = \sqrt{2}\,e^{2\,i\,t}\,[\psi_0(x,t) + \psi_1(x,t)] \tag{4}$$

where $\psi_0(x,t)$ corresponds to the quantity between square brackets in Eq. (3), and $\psi_1(x,t)$ is a small perturbation such that $|\psi_1(x,t)| \ll |\psi_0(x,t)|$. Substituting this solution in Eq. (1) and then linearizing in $\psi_1(x,t)$ by neglecting all higher order terms , we obtain

$$i\,\frac{\partial}{\partial t}\psi_1(x,t) = -\frac{1}{2}\,\frac{\partial^2}{\partial x^2}\psi_1(x,t) - 2\,\psi_0(x,t)^2\psi_1^*(x,t) - 2\,(2\,|\psi_0(x,t)|^2 - 1)\psi_1(x,t). \tag{5}$$

Expressing $\psi_1(x,t)$ in terms of its real and imaginary parts as $\psi_1(x,t) = u(x,t) + i\,v(x,t)$, the last equation gives rise to the following two coupled equations

$$\frac{\partial}{\partial t}u(x,t) = -\frac{1}{2}\,\frac{\partial^2}{\partial x^2}v(x,t) + 2\big(1 - \psi_{0r}(x,t)^2 - 3\psi_{0i}(x,t)^2\big)v(x,t) - 4\psi_{0r}(x,t)\psi_{0i}(x,t)u(x,t), \tag{6}$$

$$\frac{\partial}{\partial t}v(x,t) = \frac{1}{2}\,\frac{\partial^2}{\partial x^2}u(x,t) - 2(1 - \psi_{0i}(x,t)^2 - 3\psi_{0r}(x,t)^2)u(x,t) - 4\psi_{0r}(x,t)\psi_{0i}(x,t)v(x,t), \tag{7}$$

where ψ_{0r} and ψ_{0i} denote the real and imaginary parts of ψ_0, respectively. It is verified that these two coupled equations reproduce those associated with the MI of the CW solution with $\psi_{\mathrm{CW}}(x,t) = A\,e^{i\,A^2\,t}$ and gives rise to the well-known dispersion relation $\omega(k) = \pm\sqrt{\frac{k^2}{2}(2A^2 - \frac{k^2}{2})}$. It should be noted that in case of pulse-like solutions to the previous two equations the quantity k must be understood as an eigenmode index and not as a wavenumber, and hence $\omega(k,t)$ will not be a dispersion relation in the strict sense.

For the present case of the KMB , plane waves are not solutions to the above coupled system of equations. The time-dependence of $\psi_0(x, t)$ in the above coupled equations imposes a time-dependent dispersion $\omega(k, t)$. Defining the time and space dependencies as follows:

$$u(x,t) = U(x)\, e^{\Gamma(k,t)}, \qquad v(x,t) = V(x)\, e^{\Gamma(k,t)}, \tag{8}$$

where, for convenience, we set

$$\Gamma(k,t) = \int_0^t \omega(k,t')\, dt'. \tag{9}$$

The coupled equations take the form

$$\omega(k,t)\, U(x) = -\frac{1}{2}\frac{\partial^2}{\partial x^2} V(x) + 2(1 - \psi_{0r}(x,t)^2 - 3\psi_{0i}(x,t)^2)V(x) - 4\psi_{0r}(x,t)\psi_{0i}(x,t)U(x), \tag{10}$$

$$\omega(k,t)\, V(x) = \frac{1}{2}\frac{\partial^2}{\partial x^2} U(x) - 2(1 - \psi_{0i}(x,t)^2 - 3\psi_{0r}(x,t)^2)U(x) - 4\psi_{0r}(x,t)\psi_{0i}(x,t)V(x). \tag{11}$$

Finally, the function $\omega(k, t)$ is obtained by solving numerically this eigenvalue problem. The numerical scheme used in solving the eigensystem made of Eqs. (10) and (11) is detailed in [12].

3. Stability analysis

The MI theory, described in the previous section, is applied here to study the stability of the fundamental KMB as well as the nonautonomous KMB with periodic dispersion. With constant dispersion, we focus in Section 3.1 on the main features of the bifurcation behavior of the KMB. In Section 3.2, we study the effects of the periodic dispersion parameters on the stability of the KMB.

3.1. Bifurcation of KMB

Bifurcation of KMB is a distinguished feature by which the KMB starts at a specific time a series of bifurcations that constitute an inverted triangular shape, as shown in a number of spacio-temporal figures below, see e.g. Fig. 2. There are two bifurcation features that demand an explanation: (i) the triangular-shaped spread of the bifurcated peaks and (ii) the time at which bifurcation starts. Here we will show that it is the most unstable mode of the MI that is responsible for these two features.

We start the analysis by studying the special case of constant dispersion, namely $d_0 = 1$ and $d_1 = 0$. Since time appears in the coupled Eqs. (10) and (11), as a parameter, we diagonalize this system for a selected value of time. In the next subsection digonalization will be performed over a time interval. In Fig. 1, we show the result of diagonalizing the system (10) and (11) at $t = 0$. Fig. 1(a) shows the typical distribution of the eigenvalues in the complex plane, namely the horizontal and vertical axes correspond to oscillatory eigenmodes. A number of isolated points appear as an additional characteristic of the MI of the KMB. These correspond to pulse-like eigenmodes indicating a distinguished mechanism by which the KMB will develop instability. Performing the Fourier transformation of the eigenmodes to identify their frequency, we obtain the dispersion relation shown in Fig. 1(b). The continuous part of the dispersion relation falls exactly on that of the CW apart from the isolated points that correspond to the pulse-like eigenmodes, as described above. We note that pulse-like modes exhibit in the Fourier transform a number of frequencies among which the dominant frequency is taken to correspond to that mode.

The bifurcation feature is shown in the spacio-temporal contour plot of Fig. 2. The bifurcated peaks follow a linear trajectory, in the tx-plain, with constant slope, m, and bifurcation start-time, t_b. Our theory for explaining the bifurcation behavior is based

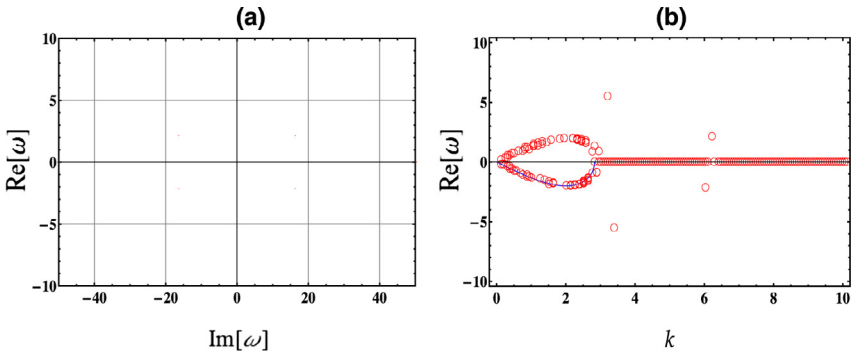

Fig. 1. (a) Real and imaginary parts of eigenvalues of the eigensystem (10) and (11) at $t = 0$. (b) Dispersion relation. The Blue curve corresponds to the CW solution. Parameters: $\phi = 0.5$, $d_0 = 1$, $d_1 = 0$. (For interpretation of the references to color in this figure legend, the reader is referred to the web version of this article).

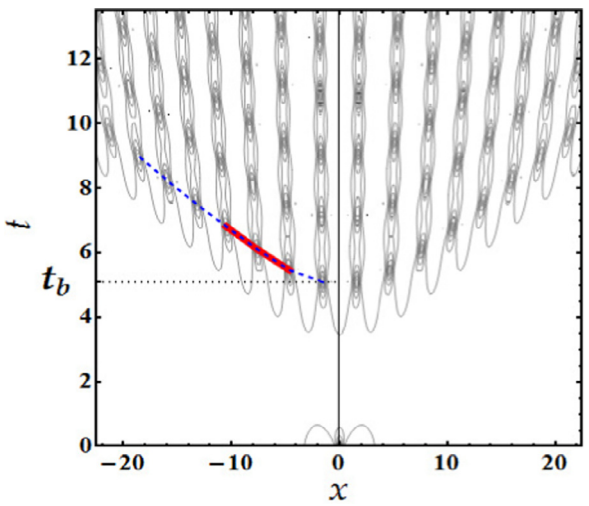

Fig. 2. Spatio-temporal contour plot of the KMB bifurcation. The plot is obtained from the numerical solution of Eq. (1) with $d(t) = 1$ and the KMB solution Eq. (3) as an initial solution. The blue dashed line connects the bifurcated peaks. The solid thick line segment is used to calculate the slope m. The bifurcation time t_b is indicated as the time when the first peak reaches its maximum. The value of $\phi = 0.01$ is used to generate this plot. (For interpretation of the references to color in this figure legend, the reader is referred to the web version of this article).

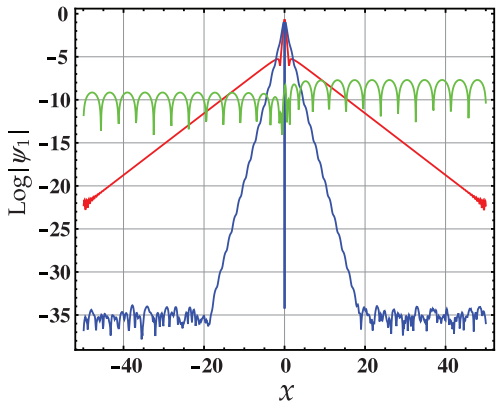

Fig. 3. Three eigenmodes corresponding to the two isolated eigenvalues of Fig. 1(a) and one eigenvalue from the continuum. The localized mode with the larger spread (red curve) corresponds to the isolated eigenvalue in the first quarter of Fig. 1(a) and the other localized mode (blue curve) corresponds to the isolated eigen value on the positive vertical axis of the same figure. The oscillatory eigenmode corresponds to an arbitrarily chosen eigenvalue from the continuum on the horizontal axis. The value of $\phi = 0.01$ is used. (For interpretation of the references to color in this figure legend, the reader is referred to the web version of this article).

on the idea that a bifurcated peak arises once the amplitude of a MI eigenmode exceeds a certain critical value. Given that all eigenmodes grow exponentially in time, the amplitude of these eigenmodes will eventually exceed, at a certain time, the critical value for bifurcation. However, the oscillatory eigenmodes extend spatially with a nondecaying envelope amplitude, as shown in Fig. 3. Had these modes been responsible for the bifurcation behavior, all bifurcated peaks should appear at the same time. The fact that the bifurcated peaks do not appear all at once but are rather generated successively, suggests that the pulse-like eigenmodes are the only possible source for such a behavior. There are two such modes corresponding to the two isolated points in Fig. 1(b), namely one in the first quarter and one on the positive vertical axis. The other isolated points correspond to degenerate eigenmodes. The profiles of these modes, which are shown in the semi-log plots of Fig. 3, acquire small-amplitude localized oscillations superposed on an envelope that decays exponentially. Since eigenmodes grow in time with $\exp(\mathrm{Re}[\omega]\, t)$ and decay spatially as $\exp(-k\,x)$, the bifurcation condition can be put mathematically as

$$\psi_1 \sim e^{\mathrm{Re}[\omega]\, t}\, e^{-k\,x} = c, \tag{12}$$

where c is a constant. Taking the logarithm, we obtain an equation for the trajectory of the peaks

$$t = m\,x + t_b, \tag{13}$$

where $m = k/\mathrm{Re}[\omega]$ is the slope of the trajectory and $t_b = \ln(c)/\mathrm{Re}[\omega]$ is another constant that corresponds to the time at which bifurcation starts.

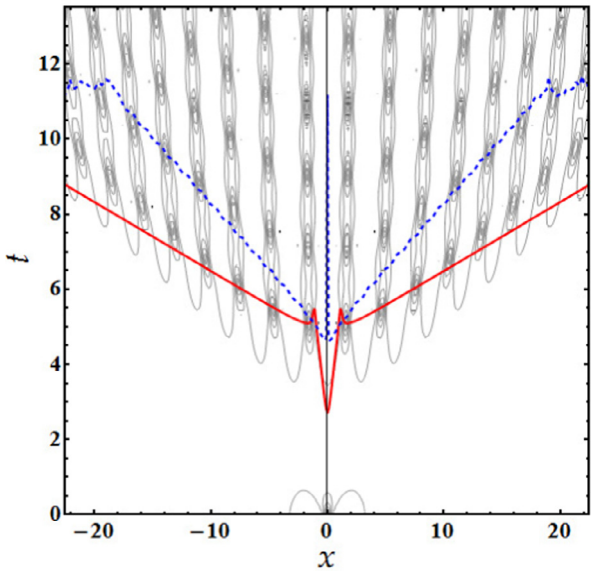

Fig. 4. Spatio-temporal contour plot of the KMB bifurcation. The plot is obtained from the numerical solution of Eq. (1) with $d(t) = 1$ and the KMB of Eq. (3) as an initial solution. The red solid curve corresponds to the localized eigenmode of the isolated eigenvalue in the first quarter of Fig. 1(a) and the dashed blue curve corresponds to the localized eigenmode of the isolated eigenvalue on the positive vertical axis of the same figure. The logarithm of both modes was taken, inverted, and then shifted by an amount that allows the first bifurcated peak to be located on the curves. The value of $\phi = 0.01$ is used. (For interpretation of the references to color in this figure legend, the reader is referred to the web version of this article).

The linear trajectory of the bifurcated peaks is verified by solving numerically the NLSE, Eq. (1) with $d(t) = 1$, as shown by the spacio-temporal contour plot of Fig. 2. Connecting the bifurcated peaks with the dashed line shows indeed a linear trajectory, apart from the first peak (closest to the vertical axis), which apparently corresponds to a transient behavior. The bifurcation time, t_b, is defined on this figure as the time at which the first peak appears. This definition is not unique since the peaks appear over a time interval. However, we considered the time at which the peak reaches its maximum value as the bifurcation time since, in this way, t_b will be determined more accurately.

To account quantitatively for the linear bifurcation trajectory, we plot the inverted logarithmic profile of the two localized eigenmodes, $-\log(|\psi_1|)/\mathrm{Re}[\omega]$, over the spacio-temporal contour plot, as shown in Fig. 4. It is expected that the linear part of the eigenmode curve fits the linear trajectory of the bifurcated peaks. By shifting the eigenmodes profiles by a constant value until the first peak is located on the curve, we find that one of the curves does account for the first five bifurcated peaks. It turns out that this eigenmode corresponds to the isolated eiegnvalue in the first quarter of the complex plane. It is clear that the other eigenmode misses most of the peaks. Therefore, we consider the former eigenmode in the analysis described below. It should be noted that this eigenmode misses the peaks near the edges of the spatial domain. We believe that this is due to the fact that MI is a linear theory which applies for short times after bifurcation. In addition, the finite size of the spacial grid does also affect the location of the peaks near the edges.

The parameter ϕ controls the frequency of peaks appearance in the KMB such that larger values of ϕ lead to larger frequency. For further quantitative account of the linear bifurcation, we perform, for a range of values of ϕ, a comparison between the slope of the linear trajectory calculated form the numerical solution of the NLSE with that of the eigenmode of the MI calculation. The slope of the trajectory of the numerical solution is calculated from the second to fourth bifurcated peaks, as shown by the solid red line segment joining the three peaks in Fig. 2. We avoided the first point since it corresponds to a transient behavior and the last few points since they will be close to the edges of the spatial grid. In Fig. 5, we plot slope-versus-ϕ curves calculated by the numerical solution for different discretizations and the corresponding curve predicted by MI. We notice that the curves show a similar trend by increasing slope with increasing ϕ.

A similar comparison would not be possible for the values of the bifurcation time, t_b, because of the unknown constant c. Nonetheless, a comparison of the trend is performed and good agreement is obtained, as shown in Fig. 6. The sharp transitions in the numerical curve correspond to the coalescence of the bifurcated peaks at $x = 0$ giving rise to a new KMB peak. Once the coalescence takes place, the numerical subroutine that searches for the bifurcated peak jumps to the next closest one which is at a finite time ahead of the disappearing one.

In the numerical solution, bifurcation is triggered by the numerical noise inevitable to avoid by any numerical technique. We conjecture that the unknown constant c that sets the bifurcation time is proportional to the amplitude of the numerical noise which in turn determines how fast will the bifurcation appear. To test this assumption, we repeated the previous calculation of the slopes and bifurcation times for decreasing values of time discretization, Δt. By decreasing Δt, the amplitude of the numerical noise will be decreased, and hence the eigenmodes will take more time to grow to the critical value for bifurcation.

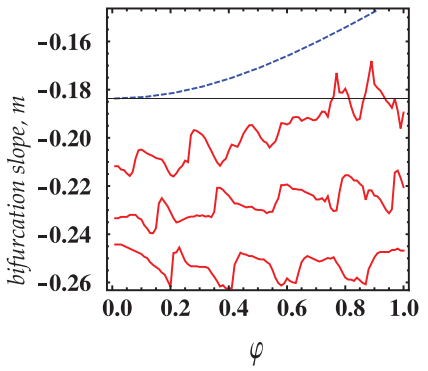

Fig. 5. Slope of bifurcated peaks trajectory versus ϕ. The three solid curves correspond, starting from the lowest, to time discretizations $\Delta t = 10^{-3}$, $\Delta t = 10^{-4}$, and $\Delta t = 10^{-5}$. The dashed curve corresponds to the slope calculated from the most unstable mode of the MI.

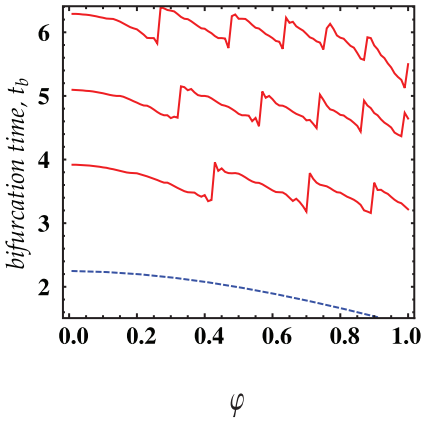

Fig. 6. Bifurcation time, t_b, versus ϕ. The three curves correspond, starting from the lowest, to time discretizations $\Delta t = 10^{-3}$, $\Delta t = 10^{-4}$, $\Delta t = 10^{-5}$. The dashed curve corresponds to the slopes calculated from the most unstable mode of the MI.

This explains the increase in t_b when Δt is decreases, as shown in Fig. 6. Furthermore, decreasing Δt enhances the agreement between the numerical and MI slopes, as shown in Fig. 5.

3.2. Periodic dispersion

Introducing the sinusoidally time-dependent perturbation on the dispersion, the MI analysis will reveal the effect of the frequency and amplitude of the perturbation on the stability of the KMB. Before we study the effect of the perturbation on stability, it is instructive to investigate how the stability of the fundamental KMB, with constant dispersion, changes with time. Performing the diagonalization of the systems (10) and (11) at different times, we obtain the trajectories of the eigen values in the complex plane, as shown in Fig. 7. From this figure, we observe that the most unstable mode, corresponding to the isolated point in the first quarter, acquires its maximum value at $t = 0.03T$ for the given set of parameters. This indicates that the KMB is most vulnerable to MI at this time. It is worth mentioning that the peak of the KMB acquires its maximum value at $t = 0$. Thus, we conclude that the KMB breather is most unstable just before or after reaching its maximum peak hight.

We turn now to the case of modulated dispersion. Solving the eigen systems (10) and (11) in the presence of the sinusoidal time-dependent dispersion, we show in Fig. 8(a) the eigenvalues at $t = 0$ for several values of modulation strengths d_1 and in Fig. 8(b) for several values of modulation frequency showing the trajectories of the isolated points. Fig. 8(b) shows that maximum MI occurs at dispersion modulation frequencies that are much larger than the natural frequency of the KMB.

To verify these findings, we compare the predictions of the MI analysis with the direct numerical solution of the NLSE. From Fig. 8(b), we conclude that MI is manipulated by the frequency of the dispersion modulation which should be apparent only for large values of ω_0. To verify this prediction, we take as the initial wavefunction the KMB exact solution and solve numerically Eq. (1) for different values of ω_0. In Fig. 9, we show the spatio-temporal density plots. Bifurcation of the KMB is considered as a sign of instability. In reference to the case of constant modulation ($\omega_0 = 0$), the bifurcation appears for the cases $\omega_0 = 80\,\Omega$ and $\omega_0 = 120\,\Omega$ at one breather period earlier than for $\omega_0 = 100\,\Omega$. This indicates that there is a parametric resonance between the oscillating dispersion and KMB around $\omega_0 = 100\,\Omega$, which is in qualitative agreement with the previous prediction based on

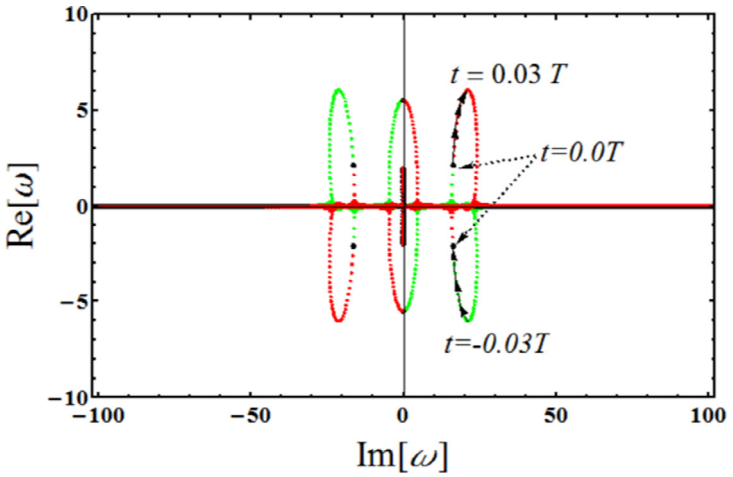

Fig. 7. Real and imaginary parts of eigenvalues of the eigensystems (10) and (11) for the time interval $t = -0.1T$ to $t = 0.1T$. At $t = 0.0T$ the 6 points in black match those of Fig. 1a. Parameters are given by: $\phi = 0.5,\ d_0 = 1\, d_1 = 0$.

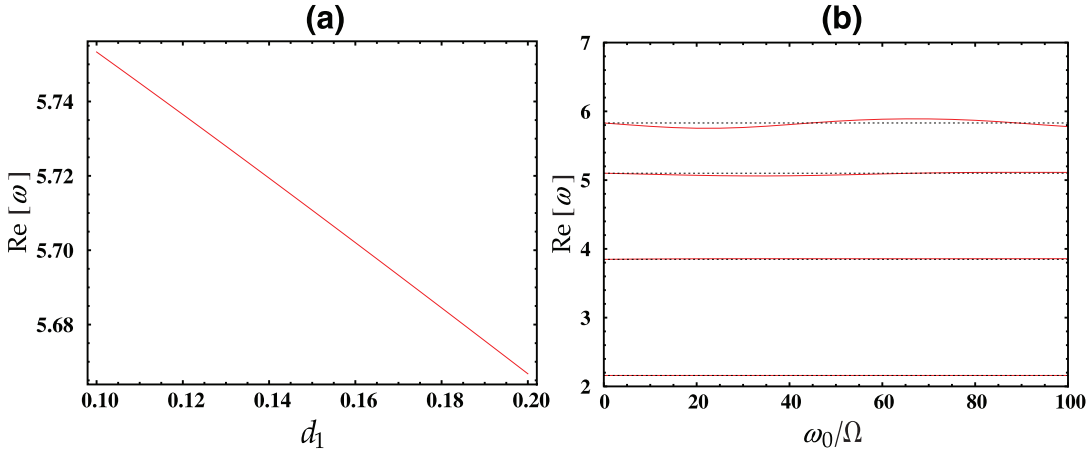

Fig. 8. Real part of eigenvalues of the eigensystems (10) and (11 for the time interval in the presence of dispersion management. The horizontal dotted lines correspond to the unperturbed case with $d_1 = 0$. Parameters: (a) $\omega_0 = 22\,\Omega$, $t = 0.03T$. (b) $d_1 = 0.1$ and $t = 0,\ 0.01\ 0.02\ 0.03$ starting from the lowest curve. The value of $\phi = 0.5$ has been used.

Fig. 8(b). It should be noted, however, that this particular value of ω_0 is not a universal one since it depends on the values of the other parameters.

From Fig. 9, we notice that the external oscillations, with frequencies $\omega \sim 100\,\Omega$, are clearly much faster than the the time scale of the pexrturbations ∼5. This, we believe, does not violate our starting assumption about the MI perturbations being faster than the natural evolution time of the KMB. This is so because the externally-oscillating dispersion is changing fast enough such that neither the KMB nor the perturbations will have time to react and an effective slowly-varying oscillation will be the dominant force acting on the breather. This conjecture is motivated by a similar behavior found by applying a high-frequency oscillation on a stationary Perigrine soliton leaving it almost unchanged [16].

It is instructive to estimate the values of the parameters of the predicted effect in view of the experiment of Ref. [10], where the KMB was realized. First, we return to the dimensional variables. We consider the propagation in an optical fiber with group velocity dispersion β_2 and nonlinearity γ. The electric field is $A = \sqrt{P_0}\psi$, the dimensional distance is $z = t\, L_{NL}$ and $T = x\, T_0$, where P_0 is the background field power and the characteristic scales are given by: $L_{NL} = 1/\gamma P_0$, $T_0 = \sqrt{|\beta_2| L_{NL}}$. In the conditions of the experiment [10] the parameters were $\beta_2 = -21.8\,\mathrm{ps}^2\,\mathrm{km}^{-1}$, $\gamma = 1.3\,\mathrm{W}^{-1}\,\mathrm{km}^{-1}$ with $P_0 = 0.7\,\mathrm{W}$ and $L_{NL} = 1.1$ km and $T_0 = 4.9$ ps. The KM periodicity was 5.3 km. For the parameter $\phi = 0.33$ (corresponding $a_{KM} = 0.5$ in the notation of [10]), we have $\Omega = 1.41$. The resonance condition gives $\omega_0 = 141$, that corresponds to modulations of dispersion with the period $l_d \approx 63$ m. Notice that in the experiment of Ref. [17], the period of modulations is around 20 m, so our estimate 63 m is experimentally accessible.

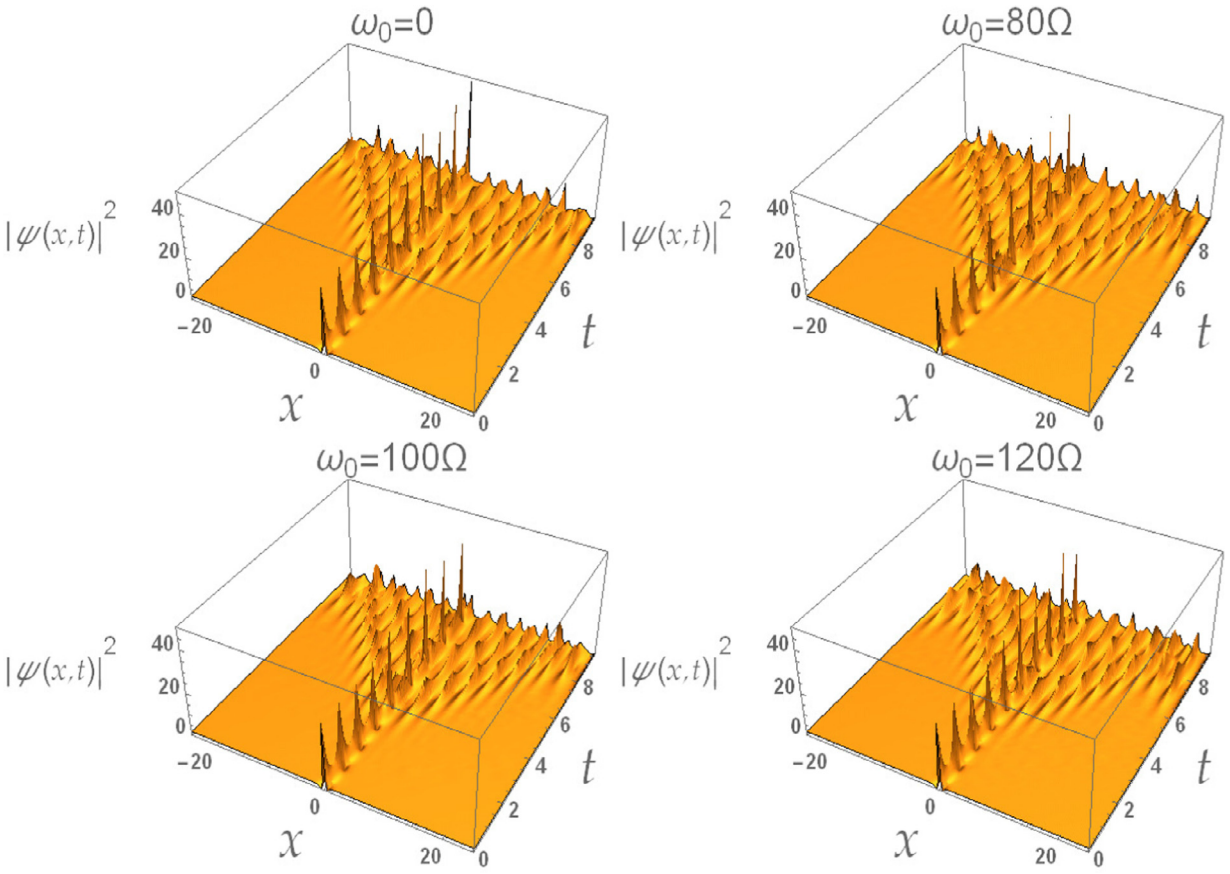

Fig. 9. Spatio-temporal plots of the KMB for different modulation frequencies. The values of parameters $\phi = 0.95$, $d_1 = 0.01$ have been used.

4. Conclusions

The MI analysis of the KMB shows that perturbations lead to bifurcation of the breather into a sequence of breathers. The analysis accounts for the distinctive bifurcation pattern and accounts quantitatively to its rate and starting time. It is shown that in a numerical solution of the relevant NLSE, the numerical noise initiates the MI perturbations, but it is the most unstable eigenmode that later dominates the time evolution. A one-to-one correspondence between the most unstable mode and the bifurcation pattern was established. In realistic situations, it is expected that bifurcation exists where it will be triggered by the small natural perturbations of the finite background.

We have also performed MI analysis to the KMB in the presence of dispersion management. Our main conclusion is that the KMB is most unstable just before and after reaching its maximum peak height. We found also that parametric resonance between the oscillating dispersion and KMB occurs at specific values that are much larger than the natural frequency of the KMB. In order to verify these predictions, we have solved numerically the NLSE with dispersion that oscillates sinusoidally where evidence for parametric resonance was indeed obtained.

Acknowledgments

The authors acknowledge support provided by King Fahd University of Petroleum and Minerals under group Project nos. RG1214-1 and RG1214-2, and the support provided the Saudi Center for Theoretical Physics (SCTP). UK acknowledges the support provided by United Arab Emirates University under the UAEU-UPAR-2013 Grant. FA acknowledges the support from Grant EDW B14-096-0981 provided by IIUM.

References

[1] Kharif C, Pelinovsky E. Eur J Mech B/Fluids 2003;22:603.
[2] Solli DR, Ropers C, Koonath P, Jalali B. Nature 2007;450:1054.
[3] Akhmediev NN, Eleonskii VM, Kulagin NE. Zh Eksp Teor Fiz 1985;89:1542 [Sov. Phys. JETP **62**, 894 (1985)].
[4] Kuznetsov EA. Dokl Aka Nauk SSSR 1977;236:575 [Sov. Phys. Dokl. **22**, 507 (1977)]; Ma Y-C. Stud Appl Math 1979;60:43.

[5] Peregrine DH, Austral J. Math Soc Ser B 1983;25:16.
[6] Shrira V, Geogjaev V. J Eng Math 2010;67:11.
[7] Chabchoub A, Hoffmann N, Akhmediev N. Phys Rev Lett 2011;106:204502.
[8] Kibler B, Fatome J, Finot C, Millot G, Dias F, Genty G, Akhmediev N, Dudley J. Nat Phys 2010;6:790.
[9] Bailung H, Sharma SK, Nakamura Y. Phys Rev Lett 2011;107:255005.
[10] Kibler B, et al. Sci Rep 2012;2:463.
[11] Akhmediev N, Soto-Crespo JM, Ankiewicz A. Phys Lett A 2009;373:2137.
[12] Khawaja UAl, Bahlouli H, Asad-uz zaman M, Al-Marzoug SM. Commun Nonlinear Sci Simul 2014;19:2706.
[13] Abdullaev FKh, Darmanyan SA, Kobyakov A, Lederer F. Phys Lett A 1996;220:213.
[14] Garnier J, Abdullaev FKh. Physica D 2000;145:65.
[15] Droques M, Kudlinski A, Bouwmans G, Martinelli G, Mussot A. Opt Lett 2012;37:4832.
[16] Khawaja UAl, Taki M. Phys Lett A 2013;377:2944.
[17] Finot C, Fatome J, Sysoliatin A, Kosolapov A, Wabnitz S. Opt Lett 2013;38:5361.